International Journal of Nanomedicine

Dovepress
Taylor & Francis Group

Open Access Full Text Article

ORIGINAL RESEARCH

GelMA@LNP/AST Promotes eNOS-Dependent Angiogenesis Through Autophagy Activation for the Treatment of Hind Limb Ischemia

Lingzhi Lai[1], Hao Wu[1], Liang Peng[2], Zhen Zhang[3], Xinfan Wu[1], Shuo Zheng[3], Zekang Su[3], Hongxing Chu[3]

[1]Maoming People's Hospital, Maoming, Guangdong, People's Republic of China; [2]The First People's Hospital of Guiyang, Guiyang, Guizhou, People's Republic of China; [3]Stomatological Hospital, School of Stomatology, Southern Medical University, Guangzhou, Guangdong, People's Republic of China

Correspondence: Hongxing Chu, Stomatological Hospital, School of Stomatology, Southern Medical University, Guangzhou, 510280, People's Republic of China, Tel +86-13533856675, Email chuhongxing22@smu.edu.cn

Purpose: Limb ischemia is a refractory disease characterized by insufficient angiogenesis and tissue necrosis. Currently, the primary clinical treatment method is surgical intervention; however, the prognosis for patients with severe limb ischemia remains unsatisfactory. Although some studies have evaluated the effects of using bioactive factors to promote neovascularization and tissue repair, the clinical outcomes have not met expectations, possibly due to the difficulties in maintaining biological activity and avoiding potential side effects. Traditional Chinese medicine, specifically astilbin (AST), is a potential therapeutic agent in promoting tissue regeneration. However, there have been no reports on its efficacy in treating limb ischemia through promoting angiogenesis.

Materials and Methods: In this study, we prepared AST-loaded lignin nanoparticles (LNP/AST) with sustained-release functionality, which were mixed with GelMA hydrogel (GelMA@LNP/AST). The angiogenic effects were evaluated in a mouse model of hind limb ischemia. To further investigate the mechanism of angiogenesis, human endothelial cell line EA.hy926 was exposed to different concentrations of AST. The effects of AST on cell migration and angiogenesis were studied using wound healing assays and angiogenesis assays. The changes in angiogenesis markers, autophagy markers, and eNOS levels were detected using qPCR and Western blotting. 3-MA was used to assess the role of autophagy in the activation of eNOS mediated by AST and its subsequent angiogenic effects.

Results: GelMA@LNP/AST significantly promoted blood flow recovery in mice with hind limb ischemia. This effect was mainly attributed to the enhanced migration and angiogenic capabilities of endothelial cells mediated by AST. A potential underlying mechanism could be that the autophagy induced by AST increases eNOS activity.

Conclusion: GelMA@LNP/AST enables complete revascularization in female mice after hind limb ischemia, thereby achieving limb preservation and restoring motor function. Given the good therapeutic potential of the GelMA@LNP/AST in revascularization, it may become an effective strategy for successfully salvaging limbs in cases of limb ischemia.

Keywords: astilbin, endothelial cells, autophagy, eNOS, angiogenesis

Introduction

Lower Limb Ischemic Disease is a serious peripheral arterial disease, affecting more than 200 million patients worldwide.[1] Typical clinical manifestations include limb coldness, intermittent claudication (pain while walking), rest pain (pain while at rest), and in severe cases, ulcers and gangrene may occur, potentially leading to amputation and death.[2,3] Surgical revascularization, which directly intervenes in the damaged vascular system (such as catheter implantation, vascular stenting, or balloon angioplasty), remains the primary treatment for this disease. However, complete cure of limb ischemia is still challenging, with limb loss rates as high as 25%.[4] The underlying cause of lower limb ischemic disease is primarily arterial ischemia and insufficient blood supply. Therefore, finding ways to

Received: 24 October 2024
Accepted: 28 January 2025
Published: 11 February 2025

promote angiogenesis and improve blood perfusion could provide new treatment strategies for lower limb ischemic disease.

Therapeutic angiogenesis has theoretically become the optimal method for treating lower limb ischemic disease. The principle involves using various techniques to transfer one or more exogenous angiogenic inducers to ischemic tissues, thereby promoting angiogenesis. These newly formed blood vessels function to compensate for the hypoxic damage caused by insufficient oxygen supply to organs and tissues due to ischemia, thus achieving the therapeutic purpose.[5–7] Therapeutic angiogenesis was first proposed by researcher Inser, whose pioneering work found that local injection of vascular endothelial growth factor (VEGF) into ischemic limbs led to the development of collateral arteries, as observed through angiography.[8] Following this study, an increasing number of scholars have used this strategy to deliver growth factors, stem cells, and bioactive molecules to ischemic tissues to increase blood flow and reduce damage caused by ischemia.[9–11]

In recent years, plant-derived natural products have received widespread attention due to their good biosafety and significant pharmacological diversity. Interestingly, both in vivo and in vitro studies have found that many natural compounds have potential angiogenic effects.[12,13] Astilbin (AST) is a flavonoid compound widely found in Sargentodoxa cuneata and some antidepressant herbs, as well as in various foods.[14] Due to its pharmacological activity and food-medicine homology, AST is considered to have great potential for clinical development. Previous studies have indicated that AST exhibits various pharmacological activities, including anti-inflammatory, immunosuppressive, antioxidant, analgesic, and antibacterial effects, demonstrating good efficacy in treating clinical conditions such as Parkinson's disease, sepsis, and wound healing.[14–17] Recent research has reported that AST has potential angiogenic effects in a zebrafish model. However, it remains unclear whether AST has potential therapeutic effects on hind limb ischemic diseases.

Autophagy is a highly conserved and essential process for the degradation and recycling of intracellular organelles and substances. It not only maintains cellular homeostasis under physiological conditions but also adapts to nutrient deprivation and other adverse environmental stresses.[18] Autophagy plays a role in vascular regeneration in various pathological conditions, such as diabetic retinopathy, tumors, and skin wound healing.[19–22] For instance, the autophagy in endothelial cells (ECs) increases under conditions of hyperthermia, hypoxia, or glucose deprivation, leading to an angiogenic phenotype characterized by enhanced cell migration and proliferation.[23–25] Recent research utilizing single-cell sequencing has explored the regulatory mechanisms of autophagy in vascular regeneration, confirming that autophagy is involved in various stages of ECs proliferation, differentiation, and migration, with its activation level depending on the metabolic state of the cells.[18] In vitro experiments have also demonstrated that inhibiting autophagy significantly suppresses the migration and tube-forming capabilities of ECs. This effect may arise because enhanced autophagy accelerates the degradation and recycling of cellular materials, providing sufficient energy for the angiogenesis process.[26] However, no studies have reported whether AST can promote angiogenesis by inducing autophagy.

In this study, to avoid the toxic side effects of AST when used at high concentrations for angiogenesis, to reduce the frequency of administration, and to alleviate patient discomfort, we selected a novel green nanoparticle, lignin (LNP), as a sustained-release carrier for AST. Research has confirmed that lignin is an excellent candidate for drug and gene delivery. Based on this, we constructed LNP/AST nanocomposites and mixed them with GelMA hydrogels to develop a sustained-release system for AST (Figure 1A). We assessed the angiogenic effects of the composite material in a mouse hind limb ischemia model and investigated the regulatory mechanisms of autophagy involved. This study is the first to demonstrate the potential angiogenic activity of AST and provides new insights into its potential therapeutic applications in the prevention or treatment of diseases associated with insufficient angiogenesis.

Materials and Methods

Preparation and Characterization of GelMA@LNP/AST

Add 6 mg of alkali lignin (AL) (Sigma, 370959) to per mL of methanol and stir magnetically for 2 hours. Then, use centrifugation to remove undissolved AL, retaining the supernatant. Gradually add 3 mL of pure water to each 1 mL of supernatant while stirring magnetically for 10 minutes. Afterward, centrifuge at 10,000 g for 10 minutes, discarding the

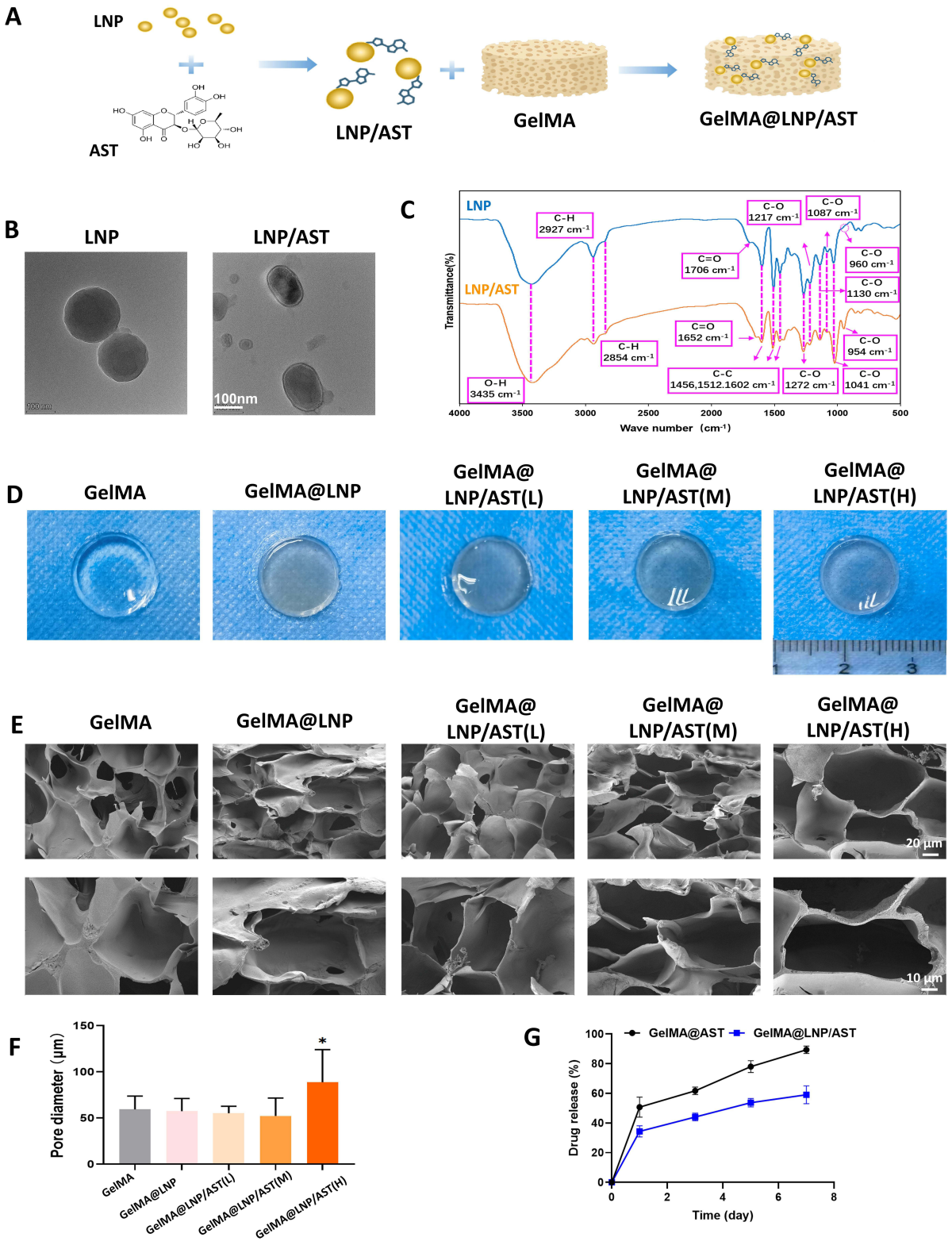

Figure 1 Characterization of GelMA@LNP/AST. (**A**) Schematic illustration of the mechanism. (**B**) TEM images of LNPs and LNP/AST. (**C**) FTIR results of LNPs and LNP/AST. (**D**) Overall images of the hydrogels from each group. (**E**) SEM results of the hydrogels from each group. (**F**) Statistical results of the pore sizes of the hydrogels shown in the images of (**E**). (**G**) Release efficiency of AST from GelMA@AST and GelMA@LNP/AST hydrogels. (*P<0.05).

https://doi.org/10.2147/IJN.S499478

supernatant. The resulting precipitate is LNPs, which are then vacuum freeze-dried for 24 hours and weighed. Resuspend LNPs in PBS to prepare a 10 mg/mL suspension, and use ultrasound to achieve uniform dispersion before adding AST (HY-N0509, MCE, US) to achieve final concentrations of 50 μM (low concentration group, GelMA@LNP/AST(L)), 500 μM (medium concentration group, GelMA@LNP/AST (M)), and 1000 μM (high concentration group, GelMA@LNP/AST(H)). Vortex for 5 minutes, and the resulting powder after freeze vacuum drying is referred to as LNP/AST. Transmission electron microscopy (TEM) is used to observe the morphology and size of LNPs and LNP/AST; Fourier-transform infrared spectroscopy (FTIR) is used to detect changes in chemical bonds. A 0.5% GelMA solution is prepared according to the manufacturer's instructions, and 5 mg of LNP/AST particles are mixed into every 1 mL of GelMA to obtain GelMA@LNP/AST. A volume of 150 μL of the GelMA hydrogel, either with or without LNP/AST particles, is subjected to light curing in a mold with an inner diameter of 1 cm for animal application. Scanning electron microscopy (SEM) is used to observe the morphology of the hydrogel, while high-performance liquid chromatography (HPLC) is employed to measure the release levels of AST on days 1, 3, 5, and 7.

Experiment on Hind Limb Ischemia

Male C57BL/6 mice aged 6–8 weeks were purchased from the Experimental Animal Center of Southern Medical University. The animal experiments in this study were in strict accordance with the Guide for the Care and Use of Laboratory Animals, and the protocols were approved by the Animal Ethics Committee of Guand Dong Hua Wei Testing Co, Ltd (Grant No.202207003). After anesthetizing with isoflurane, the superficial femoral artery and the bifurcation of the femoral artery of right side limbs were ligated and transected to establish a hind limb ischemia model. A pre-gelled hydrogel (GelMA), GelMA@LNP, GelMA@LNP/AST(L), GelMA@LNP/AST(M) or GelMA@LNP/AST(H) was placed at the site of vascular transection. The 3-methyladenine (3-MA) group received an intraperitoneal injection of 2.5 mg/kg body weight of a 3-MA solution. Immediately after surgery, as well as on days 7 and 14, laser speckle imaging (PERIMED PeriCam PSI system) was used to observe the blood flow perfusion in the lower limbs of mice in each group. The motor abilities of the mice's hind limbs were assessed on days 7 and 14.

Hematoxylin and Eosin Staining (HE) and Immunohistochemistry

On the 14th day post-surgery, gastrocnemius and thigh muscle tissues from each group of mice were collected and fixed in 4% paraformaldehyde for 2 to 3 days. The tissues were dehydrated and embedded in paraffin. After dewaxing and washing, the samples were stained with HE. Following dehydration and clearing, neutral gum was used for mounting. For immunohistochemistry, the sections were baked in a 60°C oven for 3 hours. After antigen retrieval, they were blocked with 3% BSA at room temperature for 30 minutes. The sections were incubated overnight at 4°C with CD31 antibody (11265-1-AP, Proteintech, China). After washing, the secondary antibody was incubated for 60 minutes, followed by hematoxylin counterstaining and mounting. All sections were observed and photographed using an inverted microscope (Olympus IX73).

Cell Culture and Treatment

EA.hy926 cells were purchased from Procell. They were cultured in high-glucose DMEM medium (DMEM, C11995500BT, Gibco) supplemented with 10% FBS and 1% penicillin-streptomycin in a 37°C, 5% CO_2 incubator. The cells were passaged at a 1:2 ratio every 2–3 days. The cells were treated with AST at concentrations of 1 μM, 10 μM, or 20 μM for durations of 6 hours, 12 hours, or 24 hours, respectively. For the 3-MA group, 3-MA was added 2 hours prior to AST treatment for preconditioning.

Cell Viability Assay

Cells were seeded at a density of 5000 cells per well in a 96-well plate. After adhering, they were treated with AST at concentrations of 0, 1, 10, 20, and 40 μM for either 6 or 24 hours. Then, 100 μL of MTT solution (1 mg/mL) prepared in serum-free DMEM was added to each well, and the plates were incubated in the dark at 37°C for 4 hours. After incubation, the supernatant was discarded, and 150 μL of DMSO was added to each well. The plates were shaken on a horizontal shaker for 10 minutes, and the optical density (OD) was measured at 490 nm using a microplate reader. For

the live/dead cell staining, cells were seeded in a 24-well plate and treated with AST for 24 hours. The staining working solution was prepared according to the manufacturer's instructions from the live/dead cell staining kit (E-CK-A354, Elabscience, China). 200 μL of the staining solution was added to each well and incubated at 37°C for 20 minutes. Ten minutes before the end of the incubation, PI solution was added. After the staining was complete, the results were observed using a fluorescence inverted microscope (Olympus IX73).

Migration Assay

Cells were seeded in a 12-well plate and cultured in a 37°C, 5% CO_2 incubator until they reached 100% confluence. Once confluent, a yellow pipette tip was used to create a vertical scratch in the center of each well. The wells were washed three times with PBS, and the medium was replaced with complete DMEM containing 2% FBS for continued culture. Photographs were taken at 0 hours, 6 hours, 12 hours, and 24 hours using an inverted microscope, and the scratch area was measured using Image J.

Tube Formation Assay

Cells were seeded at a density of 3×10^5 cells per well in a six-well plate. After the cells adhered, they were treated with medium containing or lacking AST for 12 hours. In a 96-well plate, 100 μL of Matrigel (356237, Corning, US) was added to each well and allowed to solidify at 37°C for 30 minutes. After AST treatment, the cells were digested with 0.25% trypsin, resuspended in ECM medium, and seeded on top of the Matrigel. After 12 hours, tube formation was observed and photographed under a microscope. The results were analyzed using Image J and the Angiogenesis Analysis plugin to assess lumen formation.

Protein Extraction and Western Blot Analysis

For animal tissue protein, the collected muscle tissue was placed in liquid nitrogen and then transferred to RIPA lysis buffer (BB-32012, Bestbio, China) supplemented with phosphatase and protease inhibitors. The tissue was homogenized using an electric homogenizer at 60 hz for 60 seconds. The homogenate was centrifuged at 12,000 rpm for 20 minutes, and the supernatant was collected as the tissue protein extract. For cells treated with AST, RIPA lysis buffer was used to lyse the cells on ice, followed by centrifugation at 12,000 rpm for 20 minutes to collect the supernatant as the cell protein extract. Loading buffer was added to both tissue and cell protein extracts, which were then heated at 99°C for 5 minutes. The prepared protein samples were separated using SDS-PAGE to differentiate proteins of various molecular weights. The proteins were transferred at a constant voltage of 110 V to a PVDF membrane (IPVH00010, Millipore, US). After a 30-minute blocking with a rapid blocking solution (PS108, EpiZime, China), the membrane was incubated overnight at 4°C with the primary antibody. After washing with TBST, the membrane was incubated at room temperature for 1 hour with the secondary antibody (ZF-0511, ZSGBbio, China). The ECL detection reagent was used for visualization, and the images obtained were analyzed for grayscale using Image J.

Immunofluorescence Staining

Cells were seeded at a density of 2×10^4 cells per well on coverslips in a 24-well plate. After adhering, the cells were treated with AST for 12 hours. They were fixed at room temperature with 4% paraformaldehyde for 30 minutes. After washing with PBS, the cells were treated with Triton X-100 (P0096, Beyotime, China) for 10 minutes, followed by blocking with 5% BSA (SW3015, Solarbio, China) at 4°C for 1 hour. The cells were incubated overnight with the LC3B antibody, and then incubated with a fluorescent secondary antibody (E-AB-1014, Elabscience, China) at room temperature for 1 hour. After sealing the slides, the samples were observed and photographed under an inverted fluorescence microscope.

Statistical Methods

Statistical analysis of all experimental data was conducted using SPSS 23.0 software. All data underwent normality tests, and results are presented as mean ± standard deviation (SD). For pairwise comparisons between groups, a *t*-test was used for statistical analysis. For multiple group comparisons, one-way analysis of variance (One-Way ANOVA) was

performed. When the data met the assumption of equal variances, the LSD post-hoc test was applied; for data with unequal variances, Tamhane's T2 post-hoc test was utilized. When assessing the recovery of blood perfusion in mice with hind limb ischemia, data was compared using a two-way repeated-measures ANOVA with Bonferroni's multiple comparisons test. Statistical significance was determined at $P < 0.05$.

Results

Characterization of GelMA@LNP/AST

As shown in Figure 1B, LNPs appeared as uniform spheres under TEM, with a diameter of (298.4609 ± 67.30076) nm. In contrast, the nanoparticles mixed with AST exhibited an elliptical shape and a reduced size of (108.9061 ± 24.93782) nm. FTIR analysis indicated that the peaks associated with the carbonyl groups of LNP and AST were different, with the peak at 1706 cm^{-1} for LNP being masked and the C-O absorption peak at 1041 cm^{-1} becoming stronger. This suggests that AST was successfully loaded onto the LNPs (Figure 1C). Overall images of the materials mixed with GelMA are shown in Figure 1D. Scanning electron microscopy (SEM) revealed the morphology of the hydrogels, where the GelMA@LNP/AST(H) group exhibited slightly larger pore sizes, while the pore sizes of other groups showed no significant statistical difference compared to the control group (Figure 1E and F). A comparison of GelMA@LNP/AST with GelMA@/AST indicated that the drug release rate over 7 days was approximately (89.333 ± 2.51661)% in GelMA@/AST group, while the GelMA@LNP/AST group had a release rate of (59.0000 ± 6.0000)% over the same period (Figure 1G). These results demonstrate that the incorporation of LNPs slows down the release of AST, contributing to a sustained release effect of the drug in vivo.

The Effect of GelMA@LNP/AST on Blood Flow Recovery in Mice with Hind Limb Ischemia

We observed that the GelMA group and the GelMA@LNP group of mice showed necrosis and absorption of the distal tissues in the hind limbs, while the gross photographs of the low and high concentration AST groups did not show significant tissue necrosis (Figure 2A). On postoperative days 7 and 14, the motor function of the mice in the GelMA@LNP/AST(L), GelMA@LNP/AST(M), and GelMA@LNP/AST(H) groups was higher than that of the GelMA group, but there was no significant difference among the three groups, and there was no significant difference between the GelMA@LNP group and the GelMA group (Figure 2B). We further observed the blood flow perfusion in the hind limbs of the mice in each group (Figure 2C and D). The results immediately after the surgery showed a significant decrease in blood flow perfusion in the operated limbs of all groups, indicating the successful modeling. On day 7, the blood flow perfusion in the GelMA@LNP/AST(L) and GelMA@LNP/AST(M) group showed no significant difference compared to the GelMA group, while the perfusion in the GelMA@LNP/AST(H) groups was significantly increased. On day 14, the average blood flow perfusion in the operated limb of the GelMA group reached (39.8172 ± 5.71398)%, while the blood flow perfusion in the GelMA@LNP/AST(L) group was (96.1004 ± 14.60605)%, in the GelMA@LNP/AST(M) group was (108.0599 ± 4.92946)%, and in the GelMA@LNP/AST(H) group was (89.2689 ± 12.1631)%. All GelMA@LNP/AST groups showed significant improvement in blood flow perfusion compared to the control group, and the GelMA@LNP/AST(M) group exhibited the most significant recovery compared to the low and high concentration groups ($P < 0.001$). At the same time, consistent with the motor function scores, there was no significant difference between the GelMA@LNP group and the GelMA group, indicating that the GelMA@LNP/AST can promote the recovery of blood flow perfusion in mice with hind limb ischemia, and this effect is primarily mediated by AST rather than LNPs.

GelMA@LNP/AST Promotes Angiogenesis in Mice with Hind Limb Ischemia

We further evaluated the effect of the GelMA@LNP/AST on mice with hind limb ischemia by examining classic indicators related to angiogenesis. First, histological analysis via HE staining revealed inflammatory infiltration in the thigh muscle tissue of the GelMA and GelMA@LNP groups, along with vacuolar necrosis of muscle fibers. In contrast, the GelMA@LNP/AST groups exhibited no significant inflammatory infiltration, and the muscle fibers remained intact

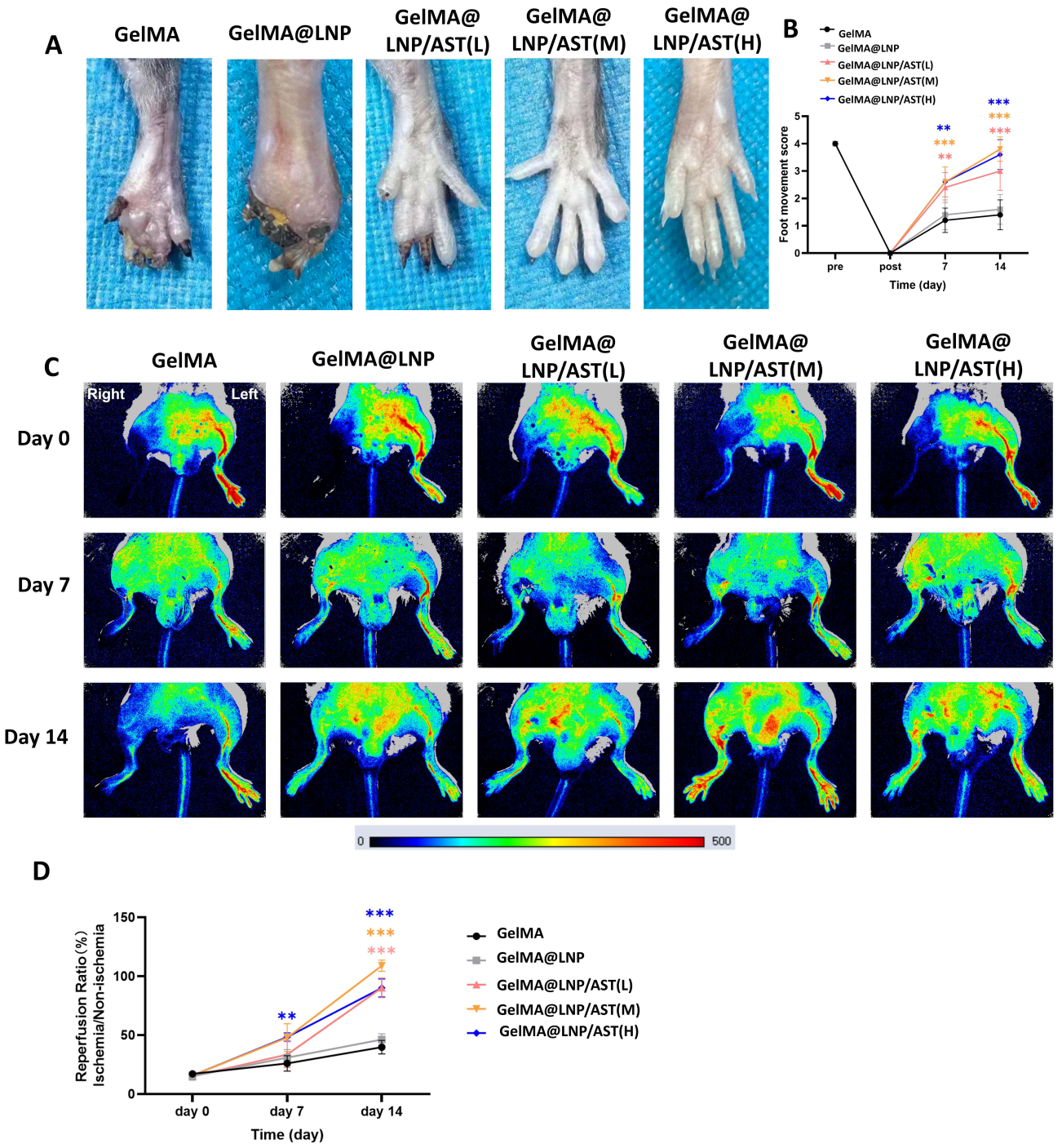

Figure 2 GelMA@LNP/AST promotes blood flow recovery in mice with hind limb ischemia. (**A**) Gross photographs of the ischemic side (right side) in mice from each group. (**B**) Hind limb functional scores of mice in each group. (**C**) Blood flow recovery in the hind limbs of mice in each group observed immediately after surgery, and at 7 and 14 days post-operation using laser speckle imaging. (**D**) Statistical results from panel C. (***P*<0.01; ****P*<0.001).

(Figure 3A). Additionally, the diameter of muscle fibers in the gastrocnemius muscle of all three GelMA@LNP/AST groups was significantly larger than that in the GelMA and GelMA@LNP groups (Figure 3A and D). Western blot analysis of VEGF and CD31 levels in the gastrocnemius muscle tissue indicated that the expression level of VEGFA in the LNP/AST group was higher than that in the GelMA group (indicated by *) and the GelMA@LNP group (indicated by #). The expression levels of CD31 in all three GelMA@LNP/AST groups were also significantly higher compared to

https://doi.org/10.2147/IJN.S499478

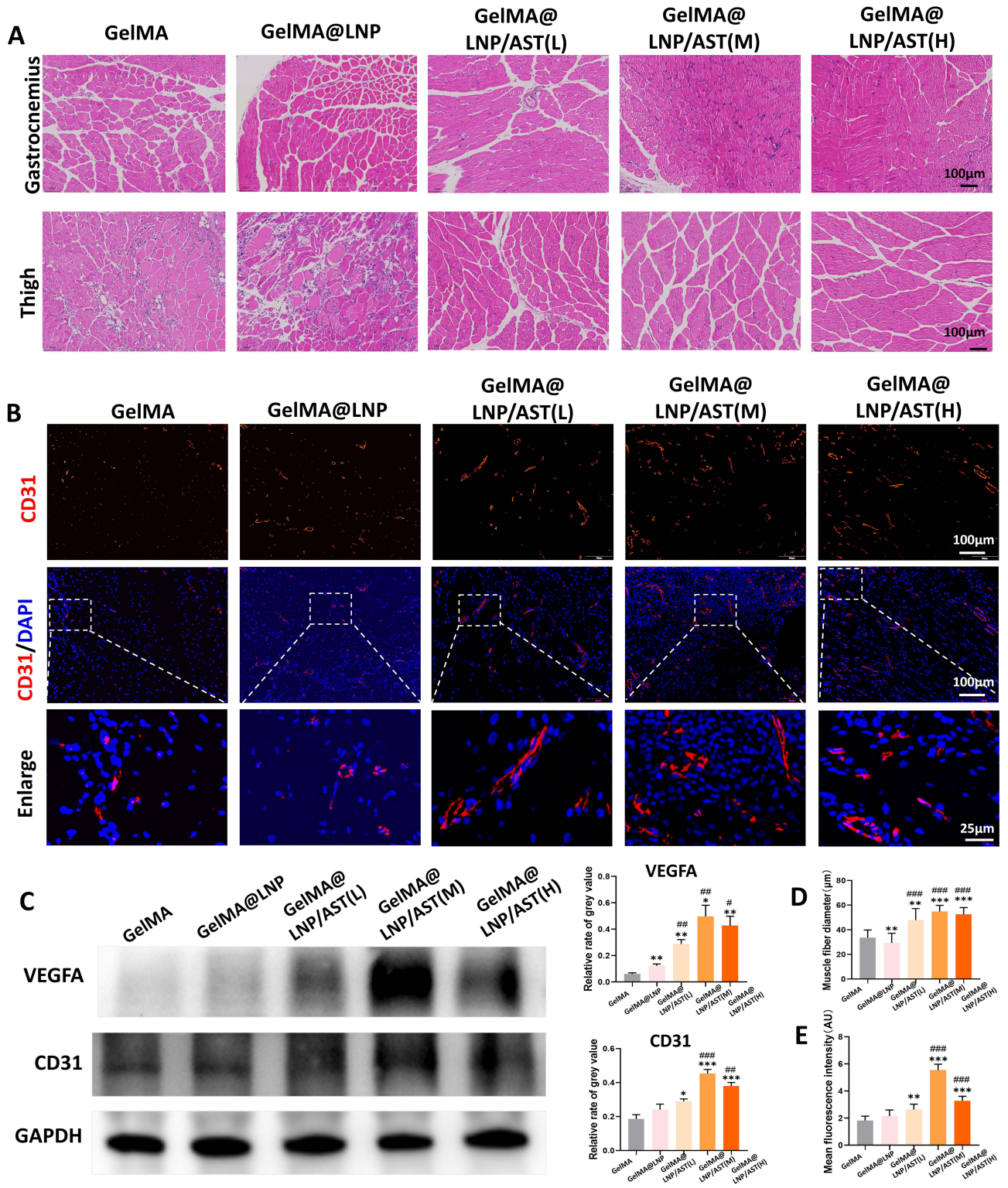

Figure 3 GelMA@LNP/AST promotes vascular regeneration in mice with hind limb ischemia. (**A**) HE staining showing the condition of the gastrocnemius and thigh muscles on the ischemic side in each group of mice. (**B**) Immunofluorescence staining showing CD31 levels in the gastrocnemius muscle. (**C**) Western blot analysis of VEGFA and CD31 levels in the gastrocnemius muscle tissue of mice. (**D**) Statistical results of the fiber diameter in the gastrocnemius muscle from panel A. (**E**) Statistical results from panel B. (Differences from the control group are indicated by *. Differences from the LNP group are indicated by $^{\#}$. * and $^{\#}P<0.05$; ** and $^{\#\#}P<0.01$; *** and $^{\#\#\#}P<0.001$).

the GelMA group, with the GelMA@LNP/AST(M) and GelMA@LNP/AST(H) groups showing increased CD31 levels compared to the GelMA@LNP group (Figure 3C). Immunofluorescence experiments revealed consistent results, showing that CD31 levels were significantly elevated in all three GelMA@LNP/AST groups (Figure 3B and E). These results suggest that the GelMA@LNP/AST promotes angiogenesis in mice with hind limb ischemia.

Effect of AST on Endothelial Cell Viability

Next, we explored the mechanism by which AST promotes angiogenesis through in vitro experiments. To select an appropriate concentration of AST for cellular studies, we referenced previous literature and chose concentrations of 1 μM, 10 μM, 20 μM, and 40 μM AST, treating endothelial cells for 6 hours and 24 hours, respectively. The results showed that after 6 hours of treatment, AST at all concentrations had no significant effect on endothelial cell viability. However, after 24 hours of treatment, a concentration of 40 μM resulted in a decrease in endothelial cell viability compared to the control group (Figure 4A). Similar results were obtained from the live/dead cell staining experiments, where only the 40 μM group of AST led to the appearance of dead cells (Figure 4C). Based on these findings, we selected concentrations of 1 μM, 10 μM, and 20 μM for subsequent in vitro experiments.

Effect of AST on Endothelial Cell Migration

In the scratch assay, we observed that 12 hours after the scratch, the migration area in the 1 μM AST treatment group did not show a significant difference compared to the control group. However, the migration area in the 10 μM and 20 μM AST groups was significantly larger. After 24 hours, the migration area in all three AST treatment groups (1 μM, 10 μM, and 20 μM) was greater than that in the control group, indicating that AST promoted endothelial cell migration. Moreover, at both 12 hours and 24 hours, the migration ability of the 10 μM and 20 μM groups was higher than that of the 1 μM group (Figure 4D and E).

Effect of AST on Endothelial Cell Tube Formation

We further assessed the effect of AST on the tube formation ability of endothelial cells using a tube formation assay (Figure 4F). After treating the cells with different concentrations of AST for 12 hours, the endothelial cells were re-plated onto a matrigel matrix. Following another 12 hours, we observed that both the 10 μM and 20 μM groups exhibited a significantly higher number of master junctions (Figure 4G) and total branching length (Figure 4H) compared to the control group. Notably, the master junction number in the 10 μM group was more pronounced than in the 20 μM group. Additionally, the total master segment length (Figure 4I) in all three AST treatment groups was superior to that in the control group, with the 10 μM group displaying a greater length than both the 1 μM and 20 μM groups. These results indicate that treatment with AST enhances the tube formation ability of endothelial cells, with the 10 μM concentration demonstrating the most significant effect.

AST Promotes the Expression of Angiogenesis-Related Proteins in Endothelial Cells

After treating ECs with AST for 6, 12, and 24 hours, we measured the expression levels of VEGFA and CD31 proteins in the cells. At 6 hours, all three concentrations of AST induced an increase in VEGFA and CD31 protein levels in the endothelial cells (Figure 5A). After 12 hours of treatment, VEGFA was upregulated in all three concentration groups, but CD31 levels only increased in the 10 μM and 20 μM groups, with the 20 μM group showing a significantly higher level of CD31 compared to the 10 μM group (Figure 5B). After 24 hours of treatment, VEGFA was significantly upregulated in the 20 μM group, and CD31 levels were induced to increase in the 10 μM, and 20 μM groups (Figure 5C). The 10 μM group showed the most significant increase in CD31 among the three groups. These results indicate that AST can significantly induce the upregulation of angiogenesis-related proteins in ECs.

AST Activates Autophagy in Endothelial Cells

We assessed the level of autophagy activation in ECs using classical standard markers for autophagy. After 6 hours of treatment, 10 μM AST caused a slight increase in p62, while in the 20 μM group, p62 showed a significant down-regulation. Both the 10 μM and 20 μM AST groups significantly upregulated LC3 II levels (Figure 6A and G). After

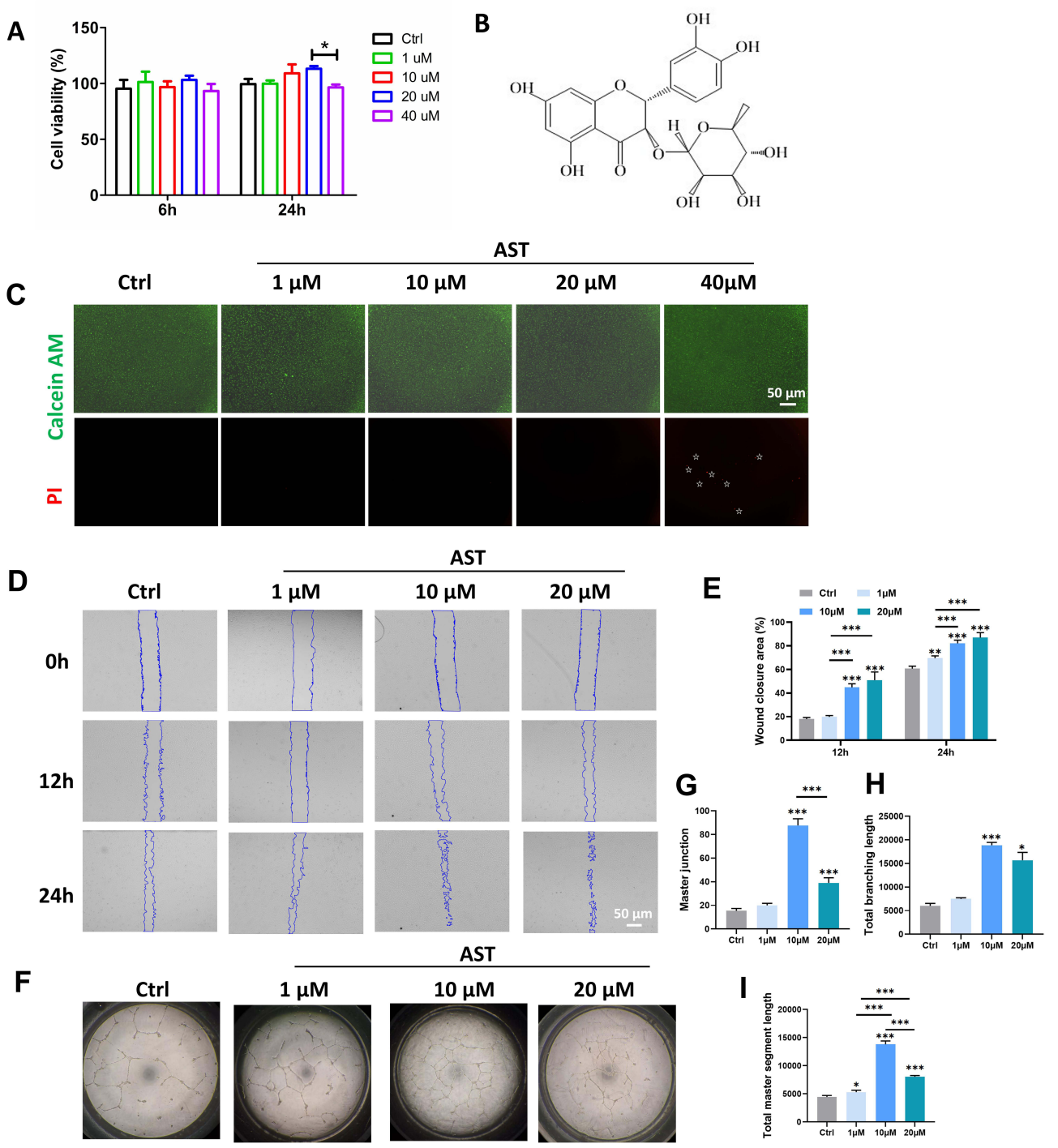

Figure 4 AST promotes endothelial cell migration and tube formation ability. (**A**) MTT assay evaluating the viability of endothelial cells treated with 1 μM, 10 μM, 20 μM, and 40 μM AST for 6 hours and 24 hours. (**B**) Chemical structure of AST. (**C**) Live/dead staining demonstrating the impact of different concentrations of AST on endothelial cell viability. (**D**) Scratch assay showing the effect of 1 μM, 10 μM, and 20 μM AST on endothelial cell migration ability. (**E**) Statistical results from panel D. (**F**) Tube formation assay evaluating the effect of 1 μM, 10 μM, and 20 μM AST on endothelial cell tube formation ability. (**G–I**) Statistical results from panel F. (*P<0.05; **P<0.01; ***P<0.001).

12 hours of treatment, p62 levels decreased in all three AST treatment groups, with LC3 II levels increasing in the 10 μM and 20 μM groups (Figure 6B and H). After 24 hours of treatment, downregulation of p62 and an increase in LC3 II levels were observed in all AST groups (Figure 6C and I). We further selected the 10 μM AST group and observed the intracellular LC3 II levels through immunofluorescence after 12 hours of treatment. The results similarly showed a significant increase in LC3 II in the AST group compared to the control group (Figure 6E and F). From the above

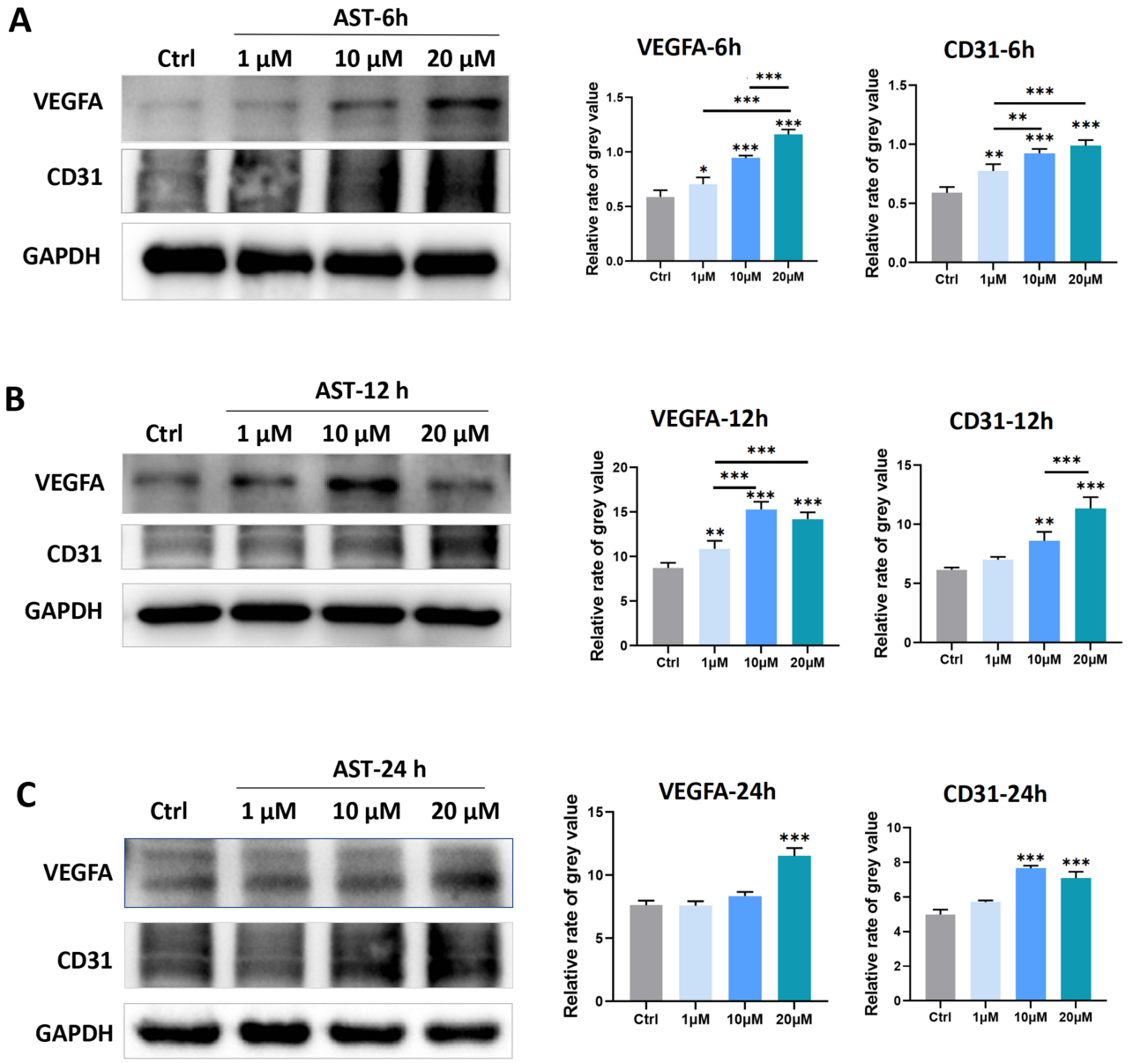

Figure 5 AST promotes the expression of angiogenesis-related proteins in endothelial cells. (**A**) Western blot analysis of VEGFA and CD31 protein levels in endothelial cells treated with 1 μM, 10 μM, and 20 μM AST for 6 hours. (**B**) Western blot analysis of VEGFA and CD31 protein levels in endothelial cells treated with 1 μM, 10 μM, and 20 μM AST for 12 hours. (**C**) Western blot analysis of VEGFA and CD31 protein levels in endothelial cells treated with 1 μM, 10 μM, and 20 μM AST for 24 hours. (**P<0.01; ***P<0.001).

results, it is clear that AST significantly induces autophagy activation in ECs. In vivo experiments yielded similar results; compared to the GelMA group and the GelMA@LNP group, the three GelMA@LNP/AST concentration groups showed significant downregulation of p62 and induction of LC3 II in the tissues (Figure 6D and J). This indicates that the addition of AST also significantly activates autophagy in vivo.

AST Induces eNOS Upregulation Through Autophagy to Promote Angiogenesis

We found that treatment with 1 μM, 10 μM, and 20 μM AST for 6 hours (Figure 7B and F), 12 hours (Figure 7C and G), and 24 hours (Figure 7D and H) significantly induced eNOS elevation in ECs in vitro. Similar results were observed in vivo, where eNOS levels in the three GelMA@LNP/AST treatment groups were significantly upregulated compared to the GelMA and GelMA@LNP groups (Figure 7E and I). eNOS is crucial for the homeostasis of normal blood vessels and the formation of new blood vessels. Additionally, there is a close relationship between eNOS and autophagy. Next,

https://doi.org/10.2147/IJN.S499478

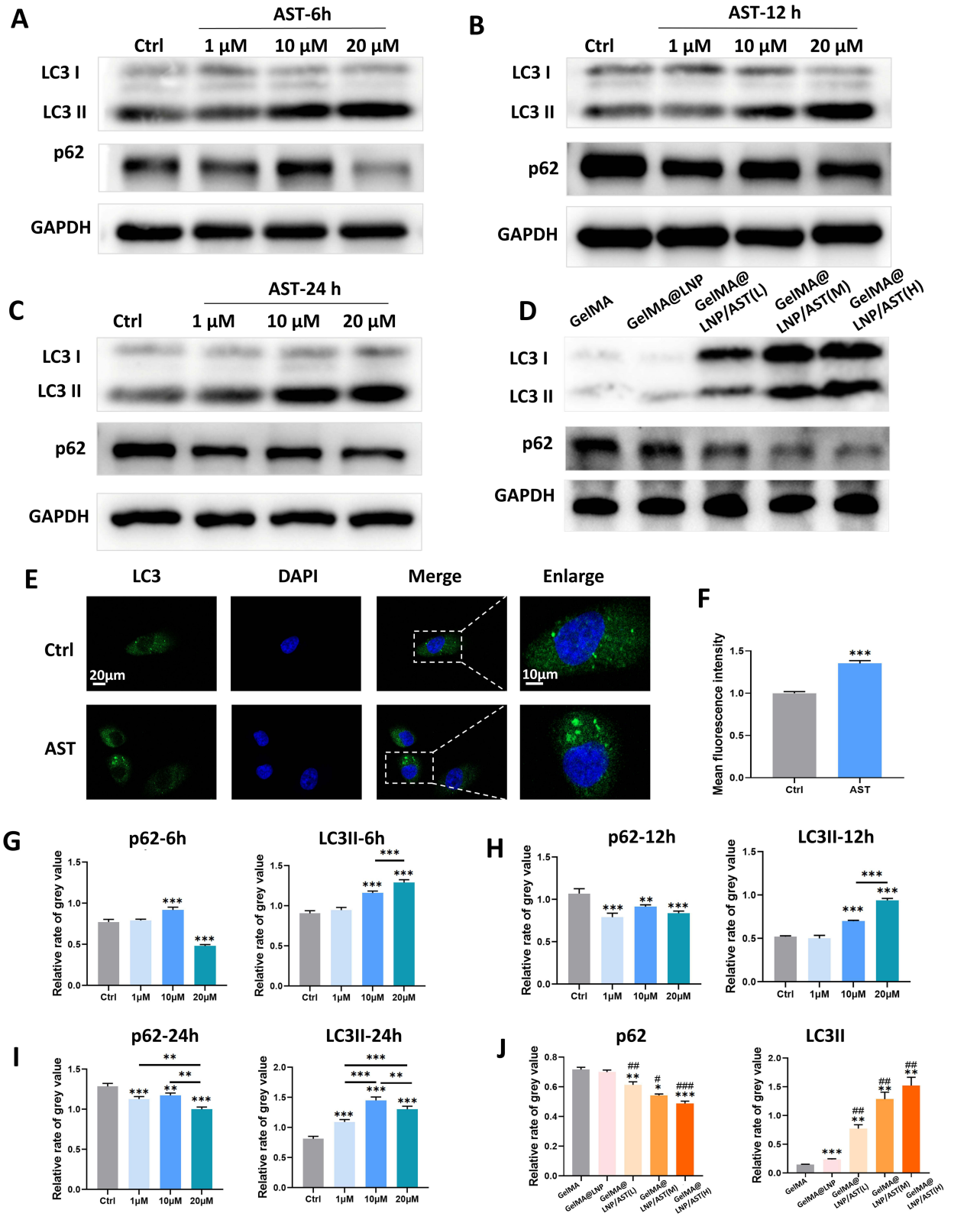

Figure 6 AST activates autophagy in endothelial cells. (**A**)–(**C**) Western blot analysis of LC3 and p62 levels in endothelial cells treated with 1 μM, 10 μM, and 20 μM AST for 6 hours, 12 hours, and 24 hours, respectively. (**D**) Western blot analysis of LC3II and p62 levels in gastrocnemius muscle tissue from mice in each group. (**E**) Immunofluorescence detection of LC3 in cells treated with 10 μM AST for 12 hours. (**F**) Statistical analysis of the results from panel E. (**G**) Statistical analysis of the results from panel A. (**H**) Statistical analysis of the results from panel B. (**I**) Statistical analysis of the results from panel C. (**J**) Statistical analysis of the results from panel D. (Differences from the control group are indicated by *. Differences from the LNP group are indicated by $^{\#}$. * and #P<0.05; ** and $^{\#\#}P$<0.01; *** and $^{\#\#\#}P$<0.001).

https://doi.org/10.2147/IJN.S499478

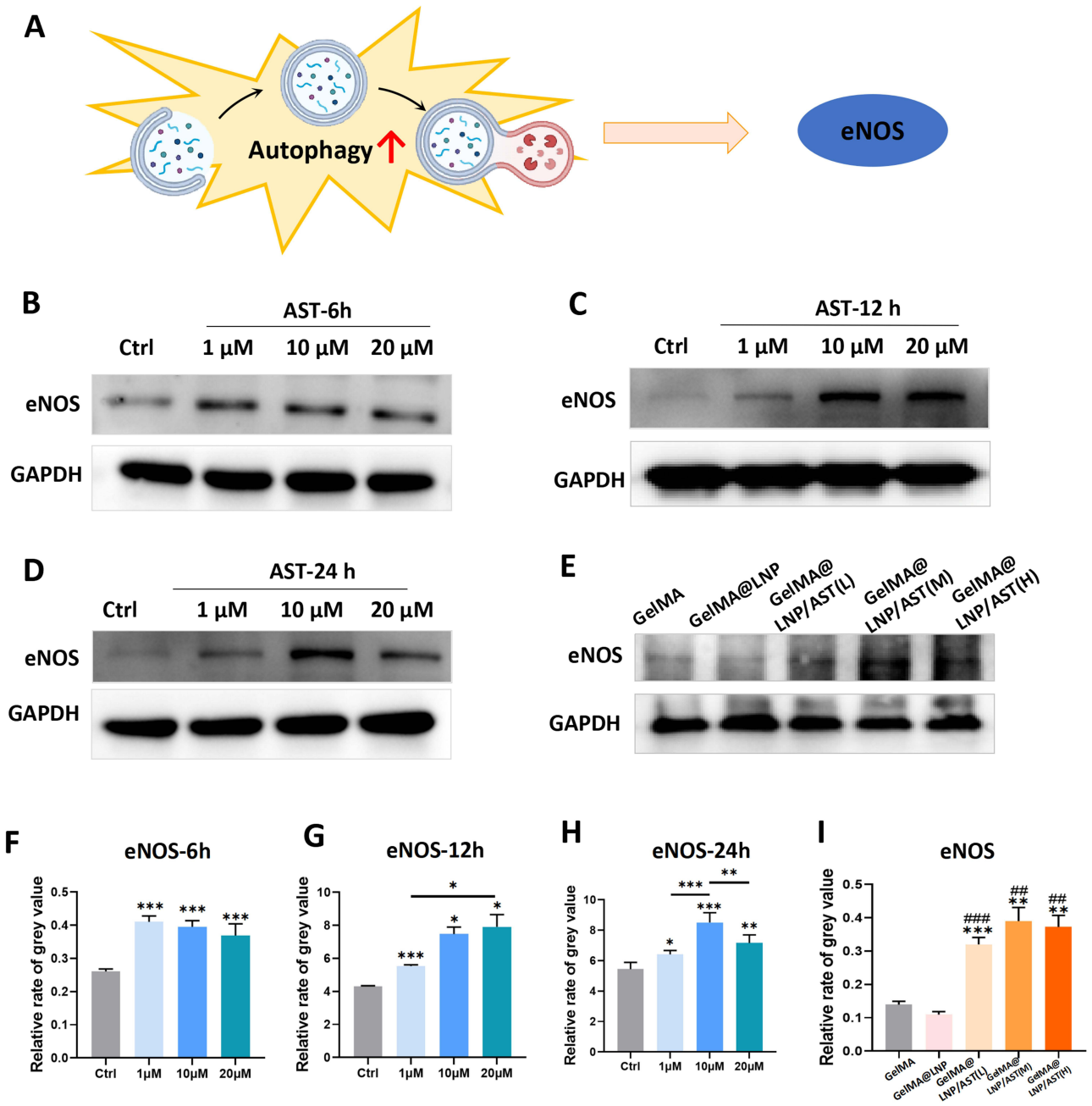

Figure 7 AST promotes the expression of eNOS in endothelial cells. (**A**) Schematic diagram of eNOS-induced autophagy activation; (**B–D**) WB detection of eNOS levels in endothelial cells treated with 1μM, 10μM, and 20μM AST for 6h, 12h, and 24h, respectively; (**E**) WB detection of eNOS levels in mouse gastrocnemius muscle; (**F**) Statistical results of Figure A; (**G**) Statistical results from panel B; (**H**) Statistical results from panel D; (**I**) Statistical results from panel E. (Differences from the control group are indicated by *. Differences from the LNP group are indicated by $^{\#}$. * and $^{\#}P<0.05$; ** and $^{\#\#}P<0.01$; *** and $^{\#\#\#}P<0.001$).

we verified whether eNOS is a key regulatory target for autophagy-induced angiogenesis. Following 3-MA treatment, the levels of eNOS and LC3 II in endothelial cells were downregulated. After combining 1 μM and 20 μM with 3-MA, the LC3 II levels showed no significant difference compared to the control, while the LC3 II levels in the 3-MA + 10 μM AST group showed only a slight increase, indicating that AST-induced autophagy was significantly inhibited by 3-MA (Figure 8A). Immunofluorescence results also suggested that AST-induced LC3 II elevation was downregulated by 3-MA (Figure 8B). At the same time, eNOS levels in the 3-MA + 1 μM and 3-MA + 10 μM groups showed no difference compared to the control, while levels in the 3-MA + 20 μM group remained lower than the control group. These results indicate that autophagy is the upstream pathway through which AST regulates eNOS. Furthermore, the VEGFA levels in

https://doi.org/10.2147/IJN.S499478

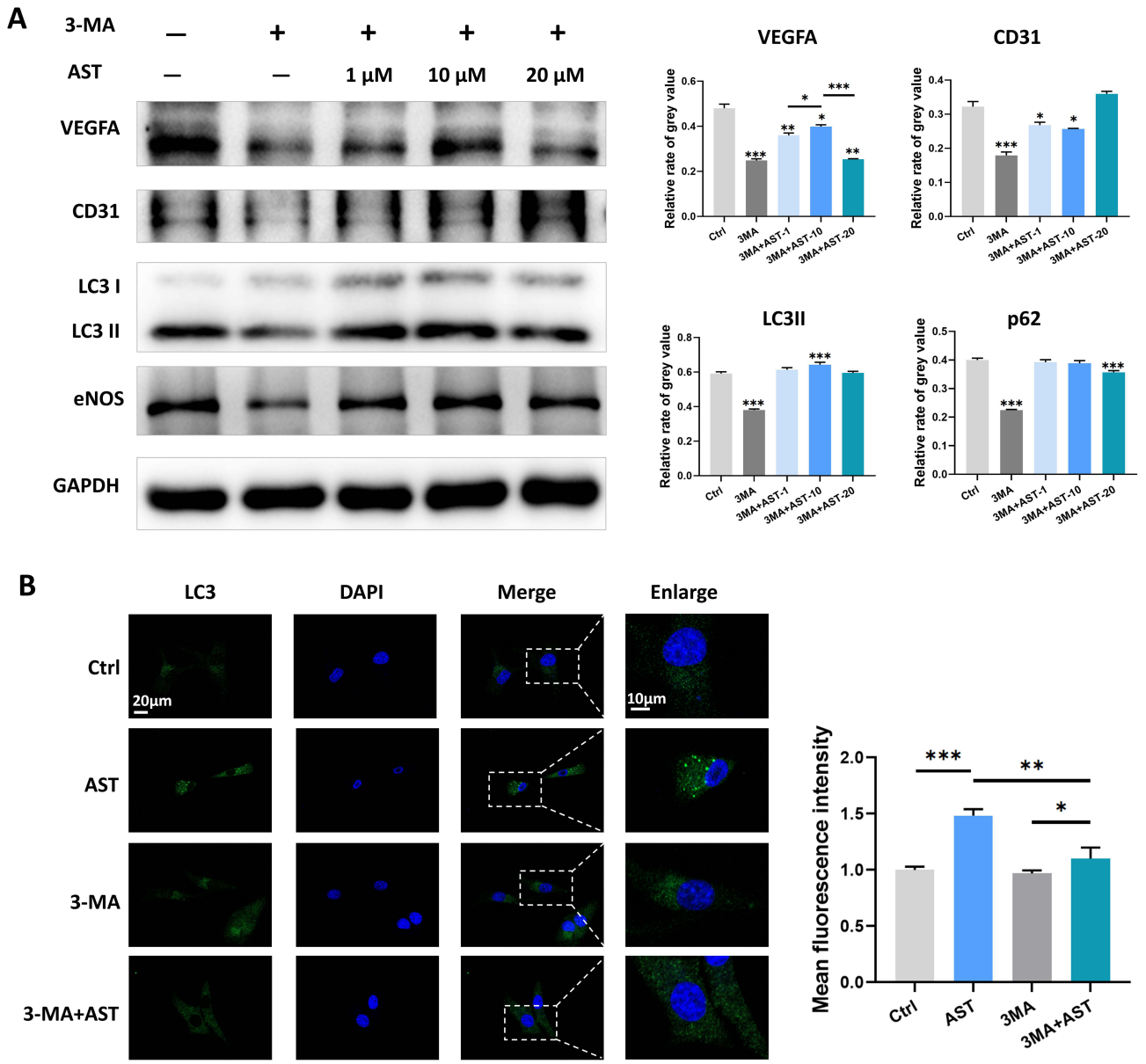

Figure 8 AST induces the expression of angiogenesis-related proteins through autophagy activation. (**A**) WB detection of angiogenesis-related proteins and autophagy-related proteins in endothelial cells after treatment with or without the 3MA inhibitor in combination with AST; (**B**) Immunofluorescence detection of LC3 in endothelial cells after treatment with or without the 3MA inhibitor in combination with AST.

the 3-MA + AST treatment group were also significantly lower than those in the control group. CD31 levels in the 3-MA + 1 μM and 3-MA + 10 μM groups showed a downward trend compared to the control, while CD31 levels in the 3-MA + 20 μM group were not significantly different from the control, suggesting that AST-induced angiogenesis was significantly inhibited when autophagy was obstructed. We drew similar conclusions from scratch assays and tube formation assays. 3-MA significantly inhibited the migratory capacity of ECs, and the promoting effect of AST on wound healing was significantly weakened when combined with 3-MA in all three AST groups (Figure 9A and B). In tube formation experiments, the master junction and total master segment length of the three AST groups combined with 3-MA were both lower than those of the control group; the total branching length in the 3-MA + 1 μM and 3-MA + 10 μM groups was also significantly downregulated compared to the control, while there was no difference between the 3-MA + 20 μM group and the control (Figure 9C–F). These results all suggest that the angiogenic capacity induced by AST is significantly inhibited by the autophagy inhibitor 3-MA.

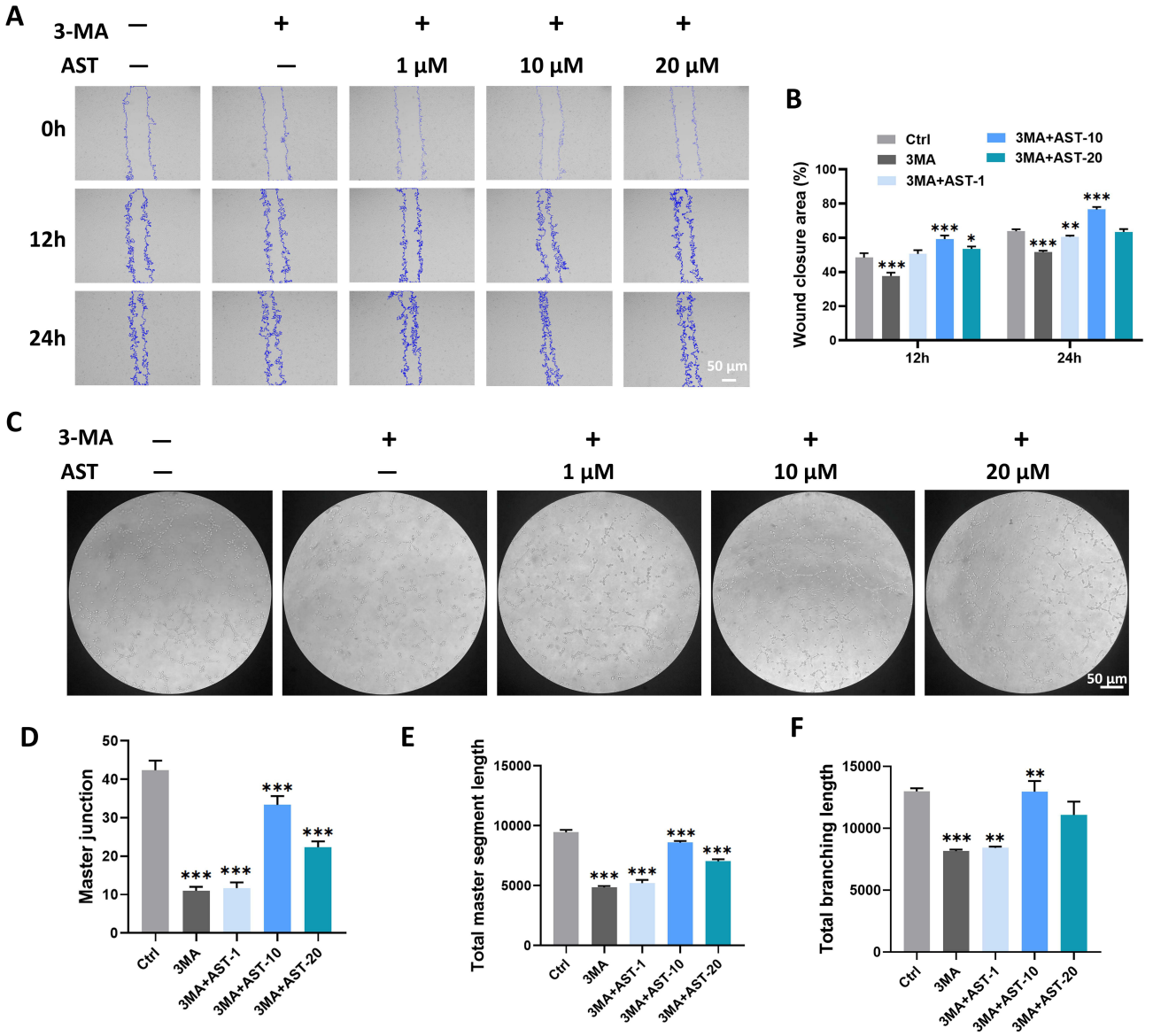

Figure 9 AST induces endothelial cell migration and tube formation through autophagy activation. (**A**) Wound healing assay to assess the migration ability of endothelial cells after treatment with or without the 3MA inhibitor in combination with AST; (**B**) Statistical results from panel A; (**C**) Tube formation assay to assess the migratory ability of endothelial cells after treatment with or without the 3MA inhibitor in combination with AST; (**D–F**) Statistical results from panel C. (*P<0.05; **P<0.01; ***P<0.001).

Similarly, in vivo experimental results indicated that the hind limb blood flow perfusion in the 3-MA + GelMA@LNP/AST group was significantly lower than that in the GelMA@LNP/AST group on postoperative days 7 and 14, suggesting that the inhibition of autophagy led to impaired blood flow perfusion recovery (Figure 10A and B). Immunofluorescence results showed that the CD31 level in the AST group was significantly induced by AST, leading to an increase in new blood vessels, while the addition of 3-MA weakened the inducing effect of AST on new blood vessels (Figure 10C and D). WB results of tissue proteins indicated that the addition of 3-MA inhibited the AST-induced increase in eNOS expression, and levels of VEGFA and CD31 were also significantly reduced (Figure 10E and F–J). These results suggest that AST can induce eNOS-dependent angiogenesis through autophagy.

Discussion

Establishing effective collateral circulation is an important therapeutic strategy for hind limb ischemia, as it provides bypass blood flow to obstructed vessels, thereby reducing the degree of damage to ischemic tissues in the hind limb.[27–29]

https://doi.org/10.2147/IJN.S499478

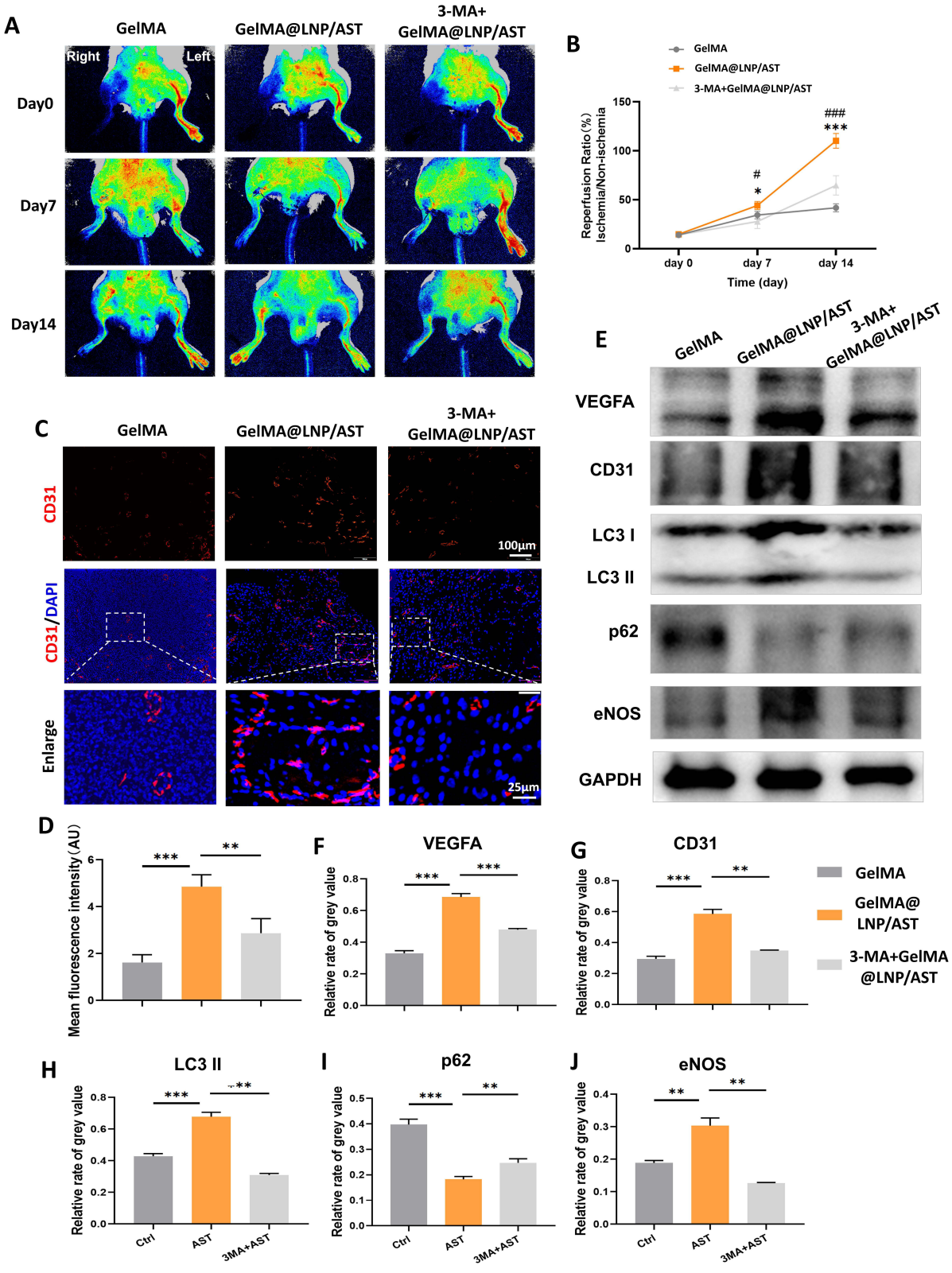

Figure 10 GelMA@LNP/AST induces blood flow recovery in ischemic hind limb mice through autophagy activation. (**A**) Blood flow assessment in the hind limbs of mice in each group immediately after surgery, and on postoperative days 7 and 14, observed using blood flow perfusion imaging with or without the 3MA inhibitor in combination with AST; (**B**) Statistical results from panel A (* suggests the difference between GelMA@LNP/AST group and GelMA group, # suggests the difference between 3-MA +GelMA@LNP/AST and GelMA@LNP/AST group); (**C**) Immunofluorescence detection of CD31 in mouse gastrocnemius muscle tissue; (**D**) Statistical results from panel C; (**E**) WB detection of angiogenesis-related proteins, autophagy-related proteins, and eNOS levels in the gastrocnemius muscle tissue of control, AST, and 3MA+AST group mice; (**F–J**) Statistical results from panel E. (* and #P<0.05; ** and $^{\#\#}P$<0.01; *** and $^{\#\#\#}P$<0.001).

Angiogenesis plays a key role in establishing collateral circulation, improving local blood supply and oxygenation in ischemic tissues.[2,4,30] ECs are important functional cells associated with angiogenesis and are the target cells in most angiogenesis-related studies. Promoting the proliferation, migration, and tube formation ability of endothelial cells is crucial for angiogenesis.[31–33] Many traditional Chinese medicine formulations, herbal extracts, and compounds are believed to have "blood-activating" functions, and some beneficial effects of these traditional medicines on the vascular system have been supported by modern medical theories.[26,34–36] AST is a dihydroflavonol compound that has been found to be widely present in various traditional herbs and foods.[37] Research has confirmed that it promotes VEGF expression and accelerates wound healing; however, its effects on angiogenesis require further investigation.[38] In this study, we prepared a slow-release system for AST to use in a hind limb ischemia model. The results showed that AST significantly enhances ECs migration and tube formation ability by promoting autophagy and activating eNOS, accelerating the rate of vascular regeneration in the ischemic area of the hind limb. This suggests that AST has good angiogenic capabilities and has the potential to become a new drug for vascular regenerative diseases.

First, we demonstrated the in vivo angiogenic effects of AST in a mouse hind limb ischemia model. Existing literature and our results indicate that high concentrations of AST can cause toxicity.[39,40] Therefore, to avoid excessively high drug concentrations in the body, reduce the frequency of administration, and alleviate patient discomfort, it is necessary to apply a sustained-release system for continuous and appropriate dosing. In this study, we selected GelMA hydrogel as a local delivery material for AST to promote angiogenesis in the ischemic hind limb. GelMA, as a novel photosensitive hydrogel, contains inherent advantages such as arginine-glycine-aspartic acid sequences and matrix metalloproteinase target sequences, along with a porous structure, which enables effective release of bioactive molecules to tissues.[41] The observation period for healing in hind limb ischemia is generally 7–14 days; however, in our study, the release efficiency of GelMA/AST was nearly 90% within 7 days, indicating that the sustained-release effect of GelMA/AST alone is not long enough. A similar finding was reported by Ou et al, which showed that the release time for the drug and hydrogel group was significantly shorter than that of the drug and carrier and hydrogel group.[42] Therefore, to maintain therapeutic drug concentrations, we chose LNPs as a scaffold to further assist in the dispersion of AST, preparing GelMA@LNP/AST to achieve sustained-release effects. LNPs are a new type of green biodegradable nanoparticles that have been proven effective in the sustained release of various traditional Chinese medicines.[43–45] FTIR results indicated that AST was successfully loaded onto the LNPs. SEM results showed that the incorporation of high concentrations of LNP/AST slightly increased the pore size of the hydrogel, while the pore sizes of other groups did not show significant statistical differences compared to the control group. The pore morphology of the hydrogel is conducive to the dispersion of AST.

In this study, 50μM (GelMA@LNP/AST(L)), 500μM (GelMA@LNP/AST(M)), and 1000μM (GelMA@LNP/AST(H)) concentrations were applied to the ischemic area. Post-operative blood flow perfusion imaging revealed that the blood flow perfusion values of the GelMA@LNP/AST treatment group significantly improved, with GelMA@LNP/AST(M) showing the best effect, indicating that the pro-angiogenic ability of AST is not dose-dependent. After tissue ischemia, the formation of collateral blood vessels can mitigate the extent of damage in ischemic tissues of the hind limbs. Previous studies have confirmed that inflammatory responses and muscle fiber necrosis in the ischemic area are important pathological processes.[46] In our study, compared to the GelMA and GelMA@LNP groups, the GelMA@LNP/AST groups showed a relatively orderly arrangement of muscle cells and less infiltration of inflammatory cells. CD31, as a marker for endothelial cells, can reflect microvascular density. Immunohistochemical staining on day 14 also indicated a significant increase in neovascularization in the GelMA@LNP/AST groups, especially in the GelMA@LNP/ AST(M) group. Similar results were observed in WB analyses of animal tissue samples. The addition of AST significantly enhanced the ECs marker CD31 and the angiogenic indicator VEGFA. The GelMA@LNP/AST we prepared, particularly the medium concentration group, exhibited a notable pro-angiogenic effect. Moreover, there was no difference in angiogenesis between the GelMA@LNP group and the GelMA group, indicating that the pro-angiogenic effect in the composite material was due to AST.

During the process of angiogenesis, ECs are induced to form specific subtypes. Tip cells are located at the forefront of the vascular sprouts, and the radial filopodia they project guide the cells to migrate towards avascular areas. At the same time, tip cells prevent the cells behind them from becoming tip cells, forcing them to adopt a stem cell phenotype, thereby maintaining their proliferative characteristics. This function reduces the number of new vascular sprouts and enhances the efficiency of vascular regeneration.[47,48] To clarify the effects of AST on ECs, we used concentrations of 1,

10, 20, and 40 μM of AST in this study. The results showed that AST did not exhibit significant cell proliferation activity, and 40 μM of AST induced significant cytotoxicity at 24 hours. Since the aim of this study was to explore the therapeutic effects of AST, its biocompatibility is crucial, thus the concentration of 40 μM was excluded. Therefore, in subsequent experiments, concentrations of 1, 10, and 20 μM of AST were used. The lack of significant effects on proliferation suggests that AST does not possess the ability to induce differentiation of endothelial cells into a stem cell direction. Next, we investigated whether it could induce a tip cell phenotype, specifically promoting cell migration capability. We used a wound healing assay to validate the effect of AST on cell migration, and the results indicated that AST significantly accelerated the wound recovery speed. Our tube formation assay also demonstrated that, compared to the control group, AST induced longer main segment lengths, a greater number of node connections, and increased grid area. Previous studies have confirmed that 100 and 500 μM AST can effectively promote the tube formation rate of HUVECs; the differences in effective concentrations may be related to the target cells involved. Vascular endothelial growth factor (VEGF) is the molecular hub of angiogenesis and is currently considered the most specific and potent angiogenic factor, capable of providing a favorable environment for angiogenesis by regulating the expression of various angiogenic molecules.[49,50] This study found that AST significantly increased the protein expression levels of the pro-angiogenic factors VEGFA and CD31. These results suggest that AST can promote angiogenesis by increasing the expression of pro-angiogenic factors that act on endothelial cells.

Autophagy promotes the circulation of intracellular substances and is a necessary process for maintaining normal cellular activity. Regulating autophagy levels has become an important therapeutic strategy for many diseases. Increasing evidence suggests that autophagy can promote angiogenesis in endothelial cells.[23,25] It is well-known that cytoplasmic LC3 (LC3-I) is converted to the autophagosome-associated form (LC3II) through conjugation with phosphatidylethanolamine, which is a prerequisite for inducing autophagy. P62 is a key autophagy receptor that can connect cargo and autophagosomes, allowing them to enter the autolysosome for the degradation of ubiquitinated substrates. Therefore, an increase in LC3II levels and a decrease in p62 levels are both indicators of autophagic activity.[51] The results showed that, at different time points after treatment with 10 μM and 20 μM AST, the number of LC3 puncta significantly increased in ECs, while the expression of LC3II increased synchronously, and p62 decreased. Only after 6 hours of 10 μM treatment was there a slight increase in p62 expression, which then gradually decreased at 12 and 24 hours. Although an increase in p62 expression is generally considered a marker of autophagy inhibition, we often observe that autophagy activation is accompanied by an upregulation of p62 during the analysis.[52,53] One potential reason could be that p62, a stress protein, dramatically increases in response to sudden changes in the cellular environment. Under the action of high concentrations of AST, excessive autophagosomes were observed to form without timely degradation by the autolysosome. Therefore, a temporary accumulation of p62 was observed, indicating "pseudo" autophagy blockade. Overall, these results indicate that AST activates autophagy. In subsequent experiments, we explored the effect of AST-induced autophagy on angiogenesis. Consistent with current reports, our findings show that exposure to 3-MA can inhibit endothelial cell migration and tube formation, as well as reduce the expression levels of angiogenesis-related proteins, alleviating the tube-forming effect of AST. This evidence strongly suggests that autophagy is key to AST-mediated angiogenesis.

Nitric oxide (NO) is a vasoactive substance secreted by the vascular endothelial system, playing a crucial role in maintaining vascular homeostasis.[54] Nitric oxide is produced byeNOS. Studies have confirmed that the activation of eNOS is a key molecular event in stimulating angiogenesis.[55] Upon activation, eNOS mediates endothelial cell migration, angiogenesis, and the recruitment of mural cells to immature angiogenic sprouts.[56] A decrease in eNOS activity and the inhibition of NO production are associated with endothelial cell dysfunction.[57] Recently, eNOS has been reported to be regulated by levels of autophagy.[58,59] In this study, we observed that AST can significantly induce the expression of eNOS within cells. However, after autophagy inhibition with 3-MA, the eNOS expression level significantly decreased, which in turn suppressed the pro-angiogenic effect of AST. These data suggest that AST induces autophagy, which promotes angiogenesis through the activation of eNOS.

Conclusion

Based on our research, the GelMA@LNP/AST sustained-release system can promote angiogenesis in mice with hind limb ischemia, and this effect is related to autophagy. AST activates autophagy, which enhances the expression of eNOS,

thereby accelerating the migration and tube formation ability of endothelial cells. The autophagy inhibitor 3-MA suppresses angiogenesis and recovery in the ischemic area of the hind limb following autophagy inhibition. In summary, these data reveal that AST is a promising drug and elucidate the role of autophagy in its mechanism of action, providing new therapeutic strategies for hind limb ischemia and related vascular regenerative diseases.

Abbreviations

AST, astilbin; LNP, lignin; LNP/AST, AST-loaded lignin nanoparticles; ECs, endothelial cells; AL, alkali lignin; TEM, Transmission electron microscopy; FTIR, Fourier-transform infrared spectroscopy; SEM, Scanning electron microscopy; HPLC, high-performance liquid chromatography; WB, Western blot; 3-MA, 3-methyladenine; DMEM, Dulbecco's modified Eagle's medium; FBS, fetal bovine serum; NO, Nitric oxide; eNOS, endothelial nitric oxide synthase.

Acknowledgments

This work was supported by the Medical Scientific Research Foundation of Guangdong Province of China (A2024512).

Disclosure

The authors declared no conflicts of interest in this paper.

References

1. Farber A, Menard MT, Conte MS. et al. Surgery or Endovascular Therapy for Chronic Limb-Threatening Ischemia. *N Engl J Med*. 2022;387(25):2305–2316. doi:10.1056/NEJMoa2207899
2. Chung H, Choi JK, Hong C, et al. A micro-fragmented collagen gel as a cell-assembling platform for critical limb ischemia repair. *Bioact Mater*. 2024;34:80–97. doi:10.1016/j.bioactmat.2023.12.008
3. Inoue O, Goten C, Hashimuko D, et al. Single-cell transcriptomics identifies adipose tissue CD271(+) progenitors for enhanced angiogenesis in limb ischemia. *Cell Rep Med*. 2023;4(12):101337. doi:10.1016/j.xcrm.2023.101337
4. Tian X, Yan X, Zang N, et al. Injectable thermosensitive selenium-containing hydrogel as mesenchymal stem cell carrier to improve treatment efficiency in limb ischemia. *Mater Today Bio*. 2024;25:100967. doi:10.1016/j.mtbio.2024.100967
5. Annex BH. Therapeutic angiogenesis for critical limb ischaemia. *Nat Rev Cardiol*. 2013;10(7):387–396. doi:10.1038/nrcardio.2013.70
6. Iyer SR, Annex BH. Therapeutic Angiogenesis for Peripheral Artery Disease: lessons Learned in Translational Science. *JACC Basic Transl Sci*. 2017;2(5):503–512. doi:10.1016/j.jacbts.2017.07.012
7. Ko SH, Bandyk DF. Therapeutic angiogenesis for critical limb ischemia. *Semin Vasc Surg*. 2014;27(1):23–31. doi:10.1053/j.semvascsurg.2014.10.001
8. Isner JM, Pieczek A, Schainfeld R, et al. Clinical evidence of angiogenesis after arterial gene transfer of phVEGF165 in patient with ischaemic limb. *Lancet*. 1996;348(9024):370–374. doi:10.1016/s0140-6736(96)03361-2
9. Han J, Luo L, Marcelina O, Kasim V, Wu S. Therapeutic angiogenesis-based strategy for peripheral artery disease. *Theranostics*. 2022;12(11):5015–5033. doi:10.7150/thno.74785
10. Besnier M, Shantikumar S, Anwar M, et al. miR-15a/-16 Inhibit Angiogenesis by Targeting the Tie2 Coding Sequence: therapeutic Potential of a miR-15a/16 Decoy System in Limb Ischemia. *mol Ther Nucleic Acids*. 2019;17:49–62. doi:10.1016/j.omtn.2019.05.002
11. Inampudi C, Akintoye E, Ando T, Briasoulis A. Angiogenesis in peripheral arterial disease. *Curr Opin Pharmacol*. 2018;39:60–67. doi:10.1016/j.coph.2018.02.011
12. Zhang Y, Hu G, Li S, et al. Pro-angiogenic activity of astragaloside IV in HUVECs in vitro and zebrafish in vivo. *Mol Med Rep*. 2012;5(3):805–811. doi:10.3892/mmr.2011.716
13. Li J, Zhang J, Zou L, et al. Pro-angiogenic effects of Ilexsaponin A1 on human umbilical vein endothelial cells in vitro and zebrafish in vivo. *Phytomedicine*. 2017;36:229–237. doi:10.1016/j.phymed.2017.10.006
14. Sharma A, Gupta S, Chauhan S, Nair A, Sharma P. Astilbin: a promising unexplored compound with multidimensional medicinal and health benefits. *Pharmacol Res*. 2020;158:104894. doi:10.1016/j.phrs.2020.104894
15. Wang SW, Xu Y, Weng YY, et al. Astilbin ameliorates cisplatin-induced nephrotoxicity through reducing oxidative stress and inflammation. *Food Chem Toxicol*. 2018;114:227–236. doi:10.1016/j.fct.2018.02.041
16. Wang M, Zhao J, Zhang N, Chen J. Astilbin improves potassium oxonate-induced hyperuricemia and kidney injury through regulating oxidative stress and inflammation response in mice. *Biomed Pharmacother*. 2016;83:975–988. doi:10.1016/j.biopha.2016.07.025
17. Maleki SJ, Crespo JF, Cabanillas B. Anti-inflammatory effects of flavonoids. *Food Chem*. 2019;299:125124. doi:10.1016/j.foodchem.2019.125124
18. Lee S, Kim H, Kim BS, et al. Angiogenesis-on-a-chip coupled with single-cell RNA sequencing reveals spatially differential activations of autophagy along angiogenic sprouts. *Nat Commun*. 2024;15(1):230. doi:10.1038/s41467-023-44427-0
19. Debnath J, Gammoh N, Ryan KM. Autophagy and autophagy-related pathways in cancer. *Nat Rev mol Cell Biol*. 2023;24(8):560–575. doi:10.1038/s41580-023-00585-z
20. Parmar UM, Jalgaonkar MP, Kulkarni YA, Oza MJ. Autophagy-nutrient sensing pathways in diabetic complications. *Pharmacol Res*. 2022;184:106408. doi:10.1016/j.phrs.2022.106408
21. Feng L, Liang L, Zhang S, Yang J, Yue Y, Zhang X. HMGB1 downregulation in retinal pigment epithelial cells protects against diabetic retinopathy through the autophagy-lysosome pathway. *Autophagy*. 2022;18(2):320–339. doi:10.1080/15548627.2021.1926655
22. Ren H, Zhao F, Zhang Q, Huang X, Wang Z. Autophagy and skin wound healing. *Burns Trauma*. 2022;10:tkac003. doi:10.1093/burnst/tkac003

23. Li Z, Wu M, Liu S, et al. Apoptotic vesicles activate autophagy in recipient cells to induce angiogenesis and dental pulp regeneration. *Mol Ther*. 2022;30(10):3193–3208. doi:10.1016/j.ymthe.2022.05.006
24. Sprott D, Poitz DM, Korovina I, et al. Endothelial-Specific Deficiency of ATG5 (Autophagy Protein 5) Attenuates Ischemia-Related Angiogenesis. *Arterioscler Thromb Vasc Biol*. 2019;39(6):1137–1148. doi:10.1161/atvbaha.119.309973
25. Liang P, Jiang B, Li Y, et al. Autophagy promotes angiogenesis via AMPK/Akt/mTOR signaling during the recovery of heat-denatured endothelial cells. *Cell Death Dis*. 2018;9(12):1152. doi:10.1038/s41419-018-1194-5
26. Pan Y, Lin T, Shao L, et al. Lignin/Puerarin Nanoparticle-Incorporated Hydrogel Improves Angiogenesis through Puerarin-Induced Autophagy Activation. *Int J Nanomed*. 2023;18:5095–5117. doi:10.2147/ijn.S412835
27. Southerland KW, Xu Y, Peters DT, et al. Skeletal muscle regeneration failure in ischemic-damaged limbs is associated with pro-inflammatory macrophages and premature differentiation of satellite cells. *Genome Med*. 2023;15(1):95. doi:10.1186/s13073-023-01250-y
28. Yu Y, Wang S, Chen X, et al. Sulfated oligosaccharide activates endothelial Notch for inducing macrophage-associated arteriogenesis to treat ischemic diseases. *Proc Natl Acad Sci U S A*. 2023;120(46):e2307480120. doi:10.1073/pnas.2307480120
29. Boutagy NE, Sessa WC. Dynamic Protein Palmitoylation Cycling: a New Pathway Impacting Peripheral Arterial Disease? *Circ Res*. 2020;127 (2):266–268. doi:10.1161/circresaha.120.317113
30. Zhong T, Gao N, Guan Y, Liu Z, Guan J. Co-Delivery of Bioengineered Exosomes and Oxygen for Treating Critical Limb Ischemia in Diabetic Mice. *ACS Nano*. 2023;17(24):25157–25174. doi:10.1021/acsnano.3c08088
31. Alashi A, Vermillion BC, Sinusas AJ. The Potential Role of PET in the Management of Peripheral Artery Disease. *Curr Cardiol Rep*. 2023;25 (8):831–839. doi:10.1007/s11886-023-01904-8
32. Kim JJ, Park JH, Kim H, et al. Vascular regeneration and skeletal muscle repair induced by long-term exposure to SDF-1α derived from engineered mesenchymal stem cells after hindlimb ischemia. *Exp Mol Med*. 2023;55(10):2248–2259. doi:10.1038/s12276-023-01096-9
33. Guo L, Yang Q, Wei R, et al. Enhanced pericyte-endothelial interactions through NO-boosted extracellular vesicles drive revascularization in a mouse model of ischemic injury. *Nat Commun*. 2023;14(1):7334. doi:10.1038/s41467-023-43153-x
34. Chu YJ, Wang ML, Wang XB, et al. Identifying quality markers of Mailuoshutong pill against thromboangiitis obliterans based on chinmedomics strategy. *Phytomedicine*. 2022;104:154313. doi:10.1016/j.phymed.2022.154313
35. Wu S, Sun Z, Guo Z, et al. The effectiveness of blood-activating and stasis-transforming traditional Chinese medicines (BAST) in lung cancer progression-a comprehensive review. *J Ethnopharmacol*. 2023;314:116565. doi:10.1016/j.jep.2023.116565
36. Fang Z, Zhang Y, Zhao X, Jin W, Yu L. The Role of PKC and HIF-1 and the Effect of Traditional Chinese Medicinal Compounds on Cerebral Ischemia-Reperfusion Injury. *Evid Based Complement Alternat Med*. 2022;2022:1835898. doi:10.1155/2022/1835898
37. Li X, Ge M, Zhu W, et al. Protective Effects of Astilbin Against Cadmium-Induced Apoptosis in Chicken Kidneys via Endoplasmic Reticulum Stress Signaling Pathway. *Biol Trace Elem Res*. 2022;200(10):4430–4443. doi:10.1007/s12011-021-03029-x
38. Ding S, Lu G, Wang B, et al. Astilbin Activates the Reactive Oxidative Species/PPARγ Pathway to Suppress Effector CD4(+) T Cell Activities via Direct Binding With Cytochrome P450 1B1. *Front Pharmacol*. 2022;13:848957. doi:10.3389/fphar.2022.848957
39. Di TT, Ruan ZT, Zhao JX, et al. Astilbin inhibits Th17 cell differentiation and ameliorates imiquimod-induced psoriasis-like skin lesions in BALB/c mice via Jak3/Stat3 signaling pathway. *Int Immunopharmacol*. 2016;32:32–38. doi:10.1016/j.intimp.2015.12.035
40. Lv K, Ren Q, Zhang X, Zhang K, Fei J, Li T. Study of pro-angiogenic activity of astilbin on human umbilical vein endothelial cells in vitro and zebrafish in vivo. *RSC Adv*. 2019;9(40):22921–22930. doi:10.1039/c9ra01673b
41. Luo Z, Sun W, Fang J, et al. Biodegradable Gelatin Methacryloyl Microneedles for Transdermal Drug Delivery. *Adv Healthc Mater*. 2019;8(3): e1801054. doi:10.1002/adhm.201801054
42. Ou Q, Zhang S, Fu C, et al. More natural more better: triple natural anti-oxidant puerarin/ferulic acid/polydopamine incorporated hydrogel for wound healing. *J Nanobiotechnology*. 2021;19(1):237. doi:10.1186/s12951-021-00973-7
43. Júnior SV, Gravina ÉG, Moraes MCB, et al. Synthesis of an organic-inorganic composite from calcium carbonate and Kraft lignin and its use as carrier material for controlled release of semiochemical agents. *Environ Sci Pollut Res Int*. 2022;29(48):72670–72682. doi:10.1007/s11356-022-21028-w
44. Djahaniani H, Ghavidel N, Kazemian H. Green and facile synthesis of lignin/HKUST-1 as a novel hybrid biopolymer metal-organic-framework for a pH-controlled drug release system. *Int J Biol Macromol*. 2023;242(Pt 1):124627. doi:10.1016/j.ijbiomac.2023.124627
45. Zhou Y, Han Y, Li G, Xiong F, Chu F. Lignin-based fluorescence hollow nanoparticles: their preparation, characterization, and encapsulation properties for doxorubicin. *Int J Biol Macromol*. 2020;165(Pt B):2136–2142. doi:10.1016/j.ijbiomac.2020.10.092
46. Duan J, Chen Z, Liang X, et al. Engineering M2-type macrophages with a metal polyphenol network for peripheral artery disease treatment. *Free Radic Biol Med*. 2024;213:138–149. doi:10.1016/j.freeradbiomed.2024.01.014
47. Malchow J, Eberlein J, Li W, Hogan BM, Okuda KS, Helker CSM. Neural progenitor-derived Apelin controls tip cell behavior and vascular patterning. *Sci Adv*. 2024;10(27):eadk1174. doi:10.1126/sciadv.adk1174
48. Alonso F, Dong Y, Li L, et al. Fibrillin-1 regulates endothelial sprouting during angiogenesis. *Proc Natl Acad Sci U S A*. 2023;120(23): e2221742120. doi:10.1073/pnas.2221742120
49. Apte RS, Chen DS, Ferrara N. VEGF in Signaling and Disease: beyond Discovery and Development. *Cell*. 2019;176(6):1248–1264. doi:10.1016/j.cell.2019.01.021
50. Hassan N, Greve B, Espinoza-Sánchez NA, Götte M. Cell-surface heparan sulfate proteoglycans as multifunctional integrators of signaling in cancer. *Cell Signal*. 2021;77:109822. doi:10.1016/j.cellsig.2020.109822
51. Klionsky DJ, Abdalla FC, Abeliovich H, et al. Guidelines for the use and interpretation of assays for monitoring autophagy. *Autophagy*. 2012;8 (4):445–544. doi:10.4161/auto.19496
52. Xu A, Yang Y, Shao Y, Wu M, Sun Y. Activation of cannabinoid receptor type 2-induced osteogenic differentiation involves autophagy induction and p62-mediated Nrf2 deactivation. *Cell Commun Signal*. 2020;18(1):9. doi:10.1186/s12964-020-0512-6
53. Li RF, Chen G, Ren JG, et al. The adaptor protein p62 is involved in RANKL-induced autophagy and osteoclastogenesis. *J Histochem Cytochem*. 2014;62(12):879–888. doi:10.1369/0022155414551367
54. Lu YA, Jiang Y, Yang HW, Hwang J, Jeon YJ, Ryu B. Diphlorethohydroxycarmalol Isolated from Ishige okamurae Exerts Vasodilatory Effects via Calcium Signaling and PI3K/Akt/eNOS Pathway. *Int J mol Sci*. 2021;22(4). doi:10.3390/ijms22041610

55. Chen J, Huang Y, Hu X, Bian X, Nian S. Gastrodin prevents homocysteine-induced human umbilical vein endothelial cells injury via PI3K/Akt/eNOS and Nrf2/ARE pathway. *J Cell Mol Med*. 2021;25(1):345–357. doi:10.1111/jcmm.16073
56. Chen J, Cui X, Zacharek A, Roberts C, Chopp M. eNOS mediates TO90317 treatment-induced angiogenesis and functional outcome after stroke in mice. *Stroke*. 2009;40(7):2532–2538. doi:10.1161/strokeaha.108.545095
57. Qu K, Cha H, Ru Y, Que H, Xing M. Buxuhuayu decoction accelerates angiogenesis by activating the PI3K-Akt-eNOS signalling pathway in a streptozotocin-induced diabetic ulcer rat model. *J Ethnopharmacol*. 2021;273:113824. doi:10.1016/j.jep.2021.113824
58. Nivoit P, Mathivet T, Wu J, et al. Autophagy protein 5 controls flow-dependent endothelial functions. *Cell mol Life Sci*. 2023;80(8):210. doi:10.1007/s00018-023-04859-9
59. Zhang JX, Qu XL, Chu P, et al. Low shear stress induces vascular eNOS uncoupling via autophagy-mediated eNOS phosphorylation. *Biochim Biophys Acta mol Cell Res*. 2018;1865(5):709–720. doi:10.1016/j.bbamcr.2018.02.005